Optimal sensor placement in structural health monitoring using discrete optimization

2015 Smart Mater. Struct. 24 125034

(http://iopscience.iop.org/0964-1726/24/12/125034)

IOP Publishing Smart Materials and Structures
Smart Mater. Struct. 24 (2015) 125034 (16pp) doi:10.1088/0964-1726/24/12/125034

Optimal sensor placement in structural health monitoring using discrete optimization

Hao Sun and Oral Büyüköztürk[1]

Department of Civil & Environmental Engineering, MIT, Cambridge, MA 02139, USA

E-mail: haosun@mit.edu and obuyuk@mit.edu

Received 26 May 2015, revised 9 September 2015
Accepted for publication 12 October 2015
Published 12 November 2015

Abstract

The objective of optimal sensor placement (OSP) is to obtain a sensor layout that gives as much information of the dynamic system as possible in structural health monitoring (SHM). The process of OSP can be formulated as a discrete minimization (or maximization) problem with the sensor locations as the design variables, conditional on the constraint of a given sensor number. In this paper, we propose a discrete optimization scheme based on the artificial bee colony algorithm to solve the OSP problem after first transforming it into an integer optimization problem. A modal assurance criterion-oriented objective function is investigated to measure the utility of a sensor configuration in the optimization process based on the modal characteristics of a reduced order model. The reduced order model is obtained using an iterated improved reduced system technique. The constraint is handled by a penalty term added to the objective function. Three examples, including a 27 bar truss bridge, a 21-storey building at the MIT campus and the 610 m high Canton Tower, are investigated to test the applicability of the proposed algorithm to OSP. In addition, the proposed OSP algorithm is experimentally validated on a physical laboratory structure which is a three-story two-bay steel frame instrumented with triaxial accelerometers. Results indicate that the proposed method is efficient and can be potentially used in OSP in practical SHM.

Keywords: optimal sensor placement, discrete optimization, modal assurance criterion, iterated improved reduced system, structural health monitoring

(Some figures may appear in colour only in the online journal)

1. Introduction

Structural health monitoring (SHM) has become an important tool for evaluating the integrity, safety and reliability throughout the lifecycle of a structural system. Important advances in sensor and computer technologies made it possible to acquire and process a large amount of structural response data, to extract the characteristic features of the data, and to link those to the structural health condition [1]. On one hand, seismic sensors are essentially used to monitor the structural status and record the dynamic response such as accelerations, displacements, strains, etc. On the other hand, the process of data feature extraction is typically realized through system identification techniques (refer to, for example, [2–13], among others) for the purpose of structural condition evaluation. Therefore, the availability as well as the quality of the sensing data affects the success of structural feature extraction and characterization, and thus has an influence on the accuracy of structural performance evaluation. This issue is related to sensor placement on a structure in SHM.

In real applications, the structure has infinite nodes and sensors can be only placed at a finite number of locations. In general, the more sensors one places on a structure, the more detailed information one obtains to represent the structural health status. Nevertheless, in practical SHM, the number of

[1] Author to whom any correspondence should be addressed.

sensors is typically limited, subjected to issues such as the budget constraint, structural inaccessibility, etc. Therefore, given only a limited number of sensors, one needs to optimize the sensor locations so as to obtain as much information of the structural system as possible. In regard to this, the topic on optimal sensor placement (OSP) has gained great attention in the past two decades. For instance, Kammer [14] proposed a significant approach called the effective independence method for OSP of large space structures. Worden and Burrows [15] investigated fault detection and classification using neural networks and methods of combinatorial optimization. Papadimitriou [16, 17] applied the information entropy (IE) to measure the performance of a sensor configuration in OSP. Rao and Anandakumar [18] treated OSP as a combinatorial optimization problem which is solved by a hybrid particle swarm optimization (PSO) approach. Yi *et al* [19] studied multiple strategies for OSP such as the QR factorization, sequential sensor placement and genetic algorithms (GAs) for sensor location optimization. Flynn and Todd [20] proposed a Bayesin OSP approach for SHM applications within a damage detection theory framework. Chang and Pakzad [21] investigated OSP for flexible structures using multi-dimensional mode shapes. It is noted that the sensor configuration obtained through the OSP analysis can be used as a theoretical reference in practical sensor placement.

Mathematically, OSP can be formulated as a constrained optimization problem in which the variables are discrete (e.g., integers) representing the candidate sensor locations on a structure. The constraints are basically determined by the available degrees-of-freedoms (DOFs) for OSP and the equality condition of the total number of given sensors. The objective function, to be minimized or maximized, is defined to measure the utility of a sensor configuration in OSP, in terms of the Fisher information matrix (FIM) [22–24], the modal assurance criterion (MAC) [25–27], the IE [16, 28–30], etc.

Once the problem of OSP is formulated, an optimization algorithm is required to solve the discrete optimization problem. For example, Yao *et al* [22] studied sensor placement for on-orbit modal identification of a space station using GA. Guo *et al* [23] presented an improved GA with binary coding for OSP of a truss bridge through maximizing a FIM-based objective function derived from mode shape sensitivities. Lian *et al* [24] proposed a discrete PSO (DPSO) technique to select the best sensor locations, for large structures such as dams, based on the FIM weighted by the nearest neighbor index. Yi *et al* [25–27] investigated several versions of the monkey algorithm (MA) (e.g., the immune MA (IMA)) with a dual encoding mechanism to solve the OSP optimization problem through minimizing the maximum MAC off-diagonal value. Several high-rise buildings, such as the Canton Tower [26] and the Dalian World Trade Building [27], were used to test the effectiveness of the MA–OSP schemes. Chow *et al* [29] presented a GA-based optimization approach based on IE to determine the OSP configuration of a typical transmission tower for the purpose of structural model updating under laboratory conditions. Yuen and Kuok [30] proposed an efficient IE-based Bayesian algorithm for placement of multi-type sensors using a heuristic sequential optimization algorithm, in which prior distribution can be incorporated. Moreover, optimal placement of both sensor and actuator systems for SHM and structural control can be found in the work done by Cha *et al* [31, 32].

In this paper, we propose a new method, called the discrete artificial bee colony (DABC) algorithm, to solve the complex discrete optimization problem of OSP. The DABC algorithm has a good convergence efficiency and is able to locate the optimal solution effectively. This paper is organized as follows. Section 2 describes OSP as an optimization problem, in which model reduction, MAC-oriented objective function, and constraint handling technique are presented. Section 3 presents a solution process to solve the discrete optimization problem of OSP based on a DABC algorithm. Section 4 illustrates three OSP examples, namely, a 27 bar truss bridge, a 21-storey building at the MIT campus, the 610 m high Canton Tower. Section 5 presents the experimental validation of the proposed OSP algorithm on a laboratory steel frame structure. Finally, discussions and concluding remarks are presented in section 6.

2. OSP as an optimization problem

The basic idea of OSP in SHM is to identify a sensor layout, given a certain number of sensors, that gives as much information of the dynamic system as possible. To realize this objective, OSP can be formulated as an optimization problem in which one aims to minimize (or maximize) a user-defined objective function related to the dynamic characteristics of a structural system, where the sensor locations are defined as the discrete optimization variables (parameters) and the constraint is typically the given sensor number, viz.

$$\min f(\boldsymbol{\vartheta}), \tag{1a}$$

$$\text{s.t.} g(\boldsymbol{\vartheta}) = n, \tag{1b}$$

$$\boldsymbol{\vartheta}^{lb} \leqslant \boldsymbol{\vartheta} \leqslant \boldsymbol{\vartheta}^{ub}, \tag{1c}$$

$$\boldsymbol{\vartheta} \in \mathbb{Z}^{+}. \tag{1d}$$

where $\boldsymbol{\vartheta} = \{\theta_1, \theta_2, ..., \theta_n\}$ denotes the sensor locations defined by a set of integers, $f(\boldsymbol{\vartheta})$ is the objective function, $g(\boldsymbol{\vartheta})$ denotes the total number of sensor locations in the optimization process, n is the given sensor number, $\boldsymbol{\vartheta}^{lb}$ and $\boldsymbol{\vartheta}^{ub}$ represent the lower and upper bounds of $\boldsymbol{\vartheta}$, respectively, and $\mathbb{Z}^{+}$ denotes the set of positive integers.

It is noted that a reduced order model is used to calculate the system characteristics, which can be obtained by the reduction of either the full-scale or the simplified model using an iterated improved reduced system (IIRS) technique as illustrated in section 2.1. A MAC-oriented objective function is employed for OSP (see section 2.2) and the constraint is handled by a penalty function as presented in section 2.3.

2.1. Model reduction using IIRS

In OSP for structural systems, a computational (e.g., finite element (FE)) model is required to calculate the system

characteristics such as the modal properties like mode shapes. However, such a model typically has plenty of DOFs, and possible sensor locations are only selected from a subset of the total DOFs (**D**). Therefore, we employ the model reduction to develop a reduced order model for OSP, namely, the IIRS method [33].

We first define the possible locations for OSP as master DOFs denoted with **m**, and the rest locations as slave DOFs denoted with **s**. Hence, we have $\mathbf{m} \cup \mathbf{s} = \mathbf{D}$. Let us write the generalized eigenvalue problem of a *N*-DOF linear system containing the first *m* modes, with the partitioned mass and stiffness matrices and mode shapes governed by the master and slave DOFs, as follows

$$\begin{bmatrix} \mathbf{K}_{mm} & \mathbf{K}_{ms} \\ \mathbf{K}_{ms}^T & \mathbf{K}_{ss} \end{bmatrix} \begin{Bmatrix} \mathbf{\Phi}_{mm} \\ \mathbf{\Phi}_{sm} \end{Bmatrix} = \begin{bmatrix} \mathbf{M}_{mm} & \mathbf{M}_{ms} \\ \mathbf{M}_{ms}^T & \mathbf{M}_{ss} \end{bmatrix} \begin{Bmatrix} \mathbf{\Phi}_{mm} \\ \mathbf{\Phi}_{sm} \end{Bmatrix} \mathbf{\Lambda}_{mm}, \tag{2}$$

where **M** and **K** are the mass and stiffness matrices, respectively; $\mathbf{\Phi} \in \mathbb{R}^{n \times m}$ is the mass-normalized mode shape matrix; $\mathbf{\Lambda} \in \mathbb{R}^{m \times m}$ is the diagonal eigenvalue matrix consisting of the eigenvalues λ_i ($i = 1, 2, ..., m$); *m* and *s* denote the number of master and slave DOFs (e.g., the sizes of **m** and **s**), respectively, satisfying $m + s = N$. Let us denote $\mathbf{\Phi}_{sm} = \mathbf{t}\mathbf{\Phi}_{mm}$, where $\mathbf{t} \in \mathbb{R}^{s \times m}$ is a transformation matrix, substitute it into the second set of equation (2) and thus obtain

$$\mathbf{t} = -\mathbf{K}_{ss}^{-1}\mathbf{K}_{ms}^T + \mathbf{K}_{ss}^{-1}\left[\mathbf{M}_{ms}^T + \mathbf{M}_{ss}\mathbf{t}\right]\mathbf{\Phi}_{mm}\mathbf{\Lambda}_{mm}\mathbf{\Phi}_{mm}^{-1}. \tag{3}$$

The substitution of $\mathbf{\Phi} = [\mathbf{\Phi}_{mm} \ \mathbf{\Phi}_{sm}]^T = \mathbf{T}\mathbf{\Phi}_{mm}$ into equation (2), pre-multiplied by $\mathbf{T}^T$, yields

$$\mathbf{M}_R^{-1}\mathbf{K}_R = \mathbf{\Phi}_{mm}\mathbf{\Lambda}_{mm}\mathbf{\Phi}_{mm}^{-1}, \tag{4}$$

where $\mathbf{T} = [\mathbf{I} \ \mathbf{t}]^T$ and $\mathbf{I} \in \mathbb{R}^{m \times m}$; $\mathbf{M}_R$ and $\mathbf{K}_R$ are the mass and stiffness matrices of the reduced order model, namely

$$\mathbf{M}_R = \mathbf{T}^T\mathbf{M}\mathbf{T} \quad \text{and} \quad \mathbf{K}_R = \mathbf{T}^T\mathbf{K}\mathbf{T}. \tag{5}$$

The substitution of equation (4) into (3) yields

$$\mathbf{t} = -\mathbf{K}_{ss}^{-1}\mathbf{K}_{ms}^T + \mathbf{K}_{ss}^{-1}\left[\mathbf{M}_{ms}^T + \mathbf{M}_{ss}\mathbf{t}\right]\mathbf{M}_R^{-1}\mathbf{K}_R. \tag{6}$$

It is noted that equation (6) forms an implicit function with **t** as the unknown parameter which can be solved through an iterative process. Friswell *et al* [33] proposed an IIRS technique to solve for equations (5) and (6) iteratively. Noteworthy, the modal quantities (e.g., mode shapes $\mathbf{\Phi}_R$) of the reduced system can be determined via solving the eigenvalue problem defined by $\mathbf{M}_R$ and $\mathbf{K}_R$ and are then employed in OSP.

2.2. MAC-oriented objective function

The MAC has been successfully applied as the objective function to measure the utility of a sensor configuration in OSP [25–27]. The MAC is defined to measure the correlation between two mode shapes (e.g., obtained from different sources). Each component of the MAC matrix is written as follows [34], taking into account the possible sensor locations

$$\mathrm{MAC}_{ij}(\vartheta) = \frac{\left[\mathbf{\Phi}_i^T(\vartheta)\mathbf{\Phi}_j(\vartheta)\right]^2}{\left[\mathbf{\Phi}_i^T(\vartheta)\mathbf{\Phi}_i(\vartheta)\right]\left[\mathbf{\Phi}_j^T(\vartheta)\mathbf{\Phi}_j(\vartheta)\right]}, \tag{7}$$

where $\mathbf{\Phi}$ is the mode shape matrix, which is calculated from the reduced order model in this study (e.g., $\mathbf{\Phi} \equiv \mathbf{\Phi}_R$); the subscripts *i* and *j* denote the *i*th and *j*th columns of $\mathbf{\Phi}$, which are indicators for the order of selected modes. The selected mode shapes are functions of the sensor location parameter ϑ. For example, $\mathbf{\Phi}_i(\vartheta)$ represents ϑ rows of the *i*th column vector in the mode shape matrix. Only the selected values in the mode shape matrix are used for MAC calculation. Noteworthy, each component of the MAC matrix is a scalar constant in the range of [0, 1] which expresses the consistency between two selected mode shapes. If the two mode shapes are consistent, MAC has the value of 1; if the two mode shapes are orthogonal to each other, MAC takes the value of 0. Noteworthy, $\mathrm{MAC}_{ij} \equiv 1$ for the case of autocorrelation ($i = j$). For the case of $i \neq j$, a small value of the MAC off-diagonal element indicates less correlation between mode shapes of two different orders, illustrating that the two mode shapes can be distinguished from each other easily; otherwise, large off-diagonal values show that the two selected mode shapes are difficult to be distinguished [26].

In regard to OSP, we aim to obtain a sensor layout that gives the minimum off-diagonal values of the MAC matrix so that the mode shapes become easily distinguishable. We herein study two objective functions defined by the off-diagonal elements of the MAC matrix in equation (7). The first objective function is the largest off-diagonal element, given by [26]

$$f(\vartheta) \equiv f_1(\vartheta) = \max_{i \neq j} \left\{\mathrm{MAC}_{ij}(\vartheta)\right\}_{i,j=1,2,...,p}, \tag{8}$$

where *p* is the total number of selected modes for OSP. The second objective function is defined as the sum of the off-diagonal element least squares, namely

$$f(\vartheta) \equiv f_2(\vartheta) = \sum_{\substack{i=1,j=1 \\ (i \neq j)}}^{p} \left[\mathrm{MAC}_{ij}(\vartheta)\right]^2. \tag{9}$$

An OSP configuration is obtained if the minimum of the objective function is found.

2.3. Constraint handling using penalty function

The OSP formulates a discrete optimization problem, in which the sensor location parameter can be only selected from the master DOF set of a model, e.g., $\theta_i \in \{1, 2, ..., m\}$ for a reduced order model ($i = 1, 2, ..., n$). Therefore, equations (1*a*)–(1*d*) become an integer optimization problem where the candidate solutions are integers from a given set. We assume that a single DOF can only be placed with a single sensor. Since it is possible that two or more parameters are equal in the optimization process (e.g., multiple sensors are placed at the same DOF), we have to define a feasible search space to eliminate this case. This can be realized by adding a penalty function to the objective function in equation (8) or

(9), as illustrated in equation (10). If multiple sensors (say q sensors) are placed at the same DOF, we eliminate redundant sensors and treat such a DOF only installed with a single sensor. In this case, the total number of active sensors considered in the optimization process becomes $g(\boldsymbol{\vartheta}) = n - q + 1$, which does not satisfy the OSP requirement. The penalty function helps to eliminate infeasible solutions in the search space. The penalized objective function is express as

$$F(\boldsymbol{\vartheta}) = f(\boldsymbol{\vartheta}) + c[g(\boldsymbol{\vartheta}) - n]^2, \tag{10}$$

where c is a constant coefficient of the penalty term (e.g., $c = 1$ in this study). Therefore, the formulation of the integer optimization problem for OSP becomes

$$\min \ F(\boldsymbol{\vartheta}), \tag{11a}$$

$$\text{s.t. } \theta_i \in \{1, 2, ..., m\}. \tag{11b}$$

The minimum solution of $F(\boldsymbol{\vartheta})$ is then the optimal sensor configuration.

3. Solution process using discrete optimization

The OSP problem formulated in the previous section can be solved by a discrete optimization algorithm with integer variables. In this study, we propose a DABC algorithm to optimize the sensor location variables in the OSP problem.

3.1. DABC algorithm for integer optimization

The artificial bee colony (ABC) algorithm and its modified version have been presented in application to structural system identification in the previous study by Sun *et al* [7]. The basic idea behind this algorithm was inspired by simulating honey bees' foraging behavior (e.g., exploration and exploitation of 'food sources'). Three search phases were proposed, named after the type of bees and their corresponding foraging duties, viz., the Employed Phase, the Onlooker Phase and the Scout Phase [35]. Only a common number of control parameters are needed to set up the algorithm, e.g., the population size N_p, the maximum number of iterations N_{max}, the limit cycle N_{lim}. The framework of the ABC algorithm and its detailed implementation for solving inverse problems with continuous variables can be further found in [36–40].

Nevertheless, when one deals with discrete optimization problems like the integer optimization in OSP, a discrete optimization algorithm should be employed. In this paper, we present a DABC algorithm, which modifies the continuous ABC algorithm, to solve a discrete type optimization problem. Consequently, the parameter to be optimized is no longer free to vary in a continuous space but is limited to specific knots in the search space. For example, the OSP problem only considers a set of integers corresponding to possible sensor positions based on the system DOFs of a model. Thus, in the optimization process, the solution can only jump from one discrete point to another. To this end, we modify the solution initialization and solution updating procedures in ABC and obtain the discrete schemes, expressed as

$$\text{Initialization} \quad \Theta_{ki} = \theta_i^{lb} + \left\lfloor \text{rand} \cdot \left(\theta_i^{ub} - \theta_i^{lb}\right) \right\rceil, \tag{12}$$

$$\text{Updating} \quad \tilde{\Theta}_{ki} = \Theta_{ki} + \left\lfloor 2(\text{rand} - 0.5) \cdot \left(\Theta_{ki} - \Theta_{ji}\right) \right\rceil, \tag{13}$$

where $i = 1, 2, \ldots, n$; $k = 1, 2, \ldots, N_p$; $\boldsymbol{\Theta} := \left\{\boldsymbol{\vartheta}_1\ \boldsymbol{\vartheta}_2\ \ldots\ \boldsymbol{\vartheta}_{N_p}\right\}^T$ is the parameter population; $\tilde{\boldsymbol{\Theta}}$ is the updated population; j denotes the solution index in the population (j is an integer randomly selected in $[1\ N_p]$ and $j \neq k$); 'rand' denotes a uniformly distributed random number in the range of [0, 1]; and $\lfloor \cdot \rceil$ represents the nearest integer function, e.g., $\lfloor 2.4 \rceil = 2, \lfloor 2.5 \rceil = 3$ and $\lfloor 2.6 \rceil = 3$.

It can be observed that the solution updating strategy in equation (13) generates a candidate solution by performing perturbation based on a uniformly random combination of the original solution and its neighborhood. This has low efficiency because the new solution set comes from random mutation. Due to the nature of uniform randomness, the probability of generating a good solution is identical to that of generating a bad one. This is beneficial for solution exploration (global search) but is less powerful in solution exploitation (local search). Therefore, a best-solution-guided updating strategy is proposed here for generating candidate solutions, considering both the randomness and information associated with the current best solution, which has been successfully employed in solving flaw detection problems [10]. To wit, we propose a new solution updating strategy, in the proposed DABC algorithm, obtained by modifying the continuous solution updating strategy into an 'integer' version:

$$\tilde{\Theta}_{ki} = \Theta_{ki} + \left\lfloor 2(\text{rand} - 0.5) \cdot \left(\Theta_{ki} - \Theta_{ji}\right) + \text{rand} \cdot \left(\theta_i^b - \Theta_{ki}\right) \right\rceil, \tag{14}$$

where the superscript 'b' denotes the current best solution in the population. It is noteworthy that the general procedure of DABC follows the same architecture of the classic ABC algorithm (see [7]). The purpose of employing the proposed DABC algorithm in this work is to converge to a number of positions where sensors are recommended to be located.

3.2. Procedure for OSP

In summary, a FE model needs to be establisghed to implement the proposed OSP algorithm. Parameters required to set up the algorithm are given as follows: the number of DOFs of the full scale or the simplified model (N), the mass matrix ($\mathbf{M}$), the stiffness matrix ($\mathbf{K}$), the master DOFs ($\mathbf{m}$), the slave DOFs ($\mathbf{s}$), the upper and lower bounds for the sensor locations ($\boldsymbol{\vartheta}^{ub}$ and $\boldsymbol{\vartheta}^{lb}$), the number of sensors for OSP (n), the DABC population size (N_p), the maximum number of iterations N_{max}, and the limit cycle N_{lim}. The procedure for OSP in SHM using the proposed DABC algorithm is illustrated in figure 1. The corresponding detailed pseudo code is given in figure A1 in appendix A.

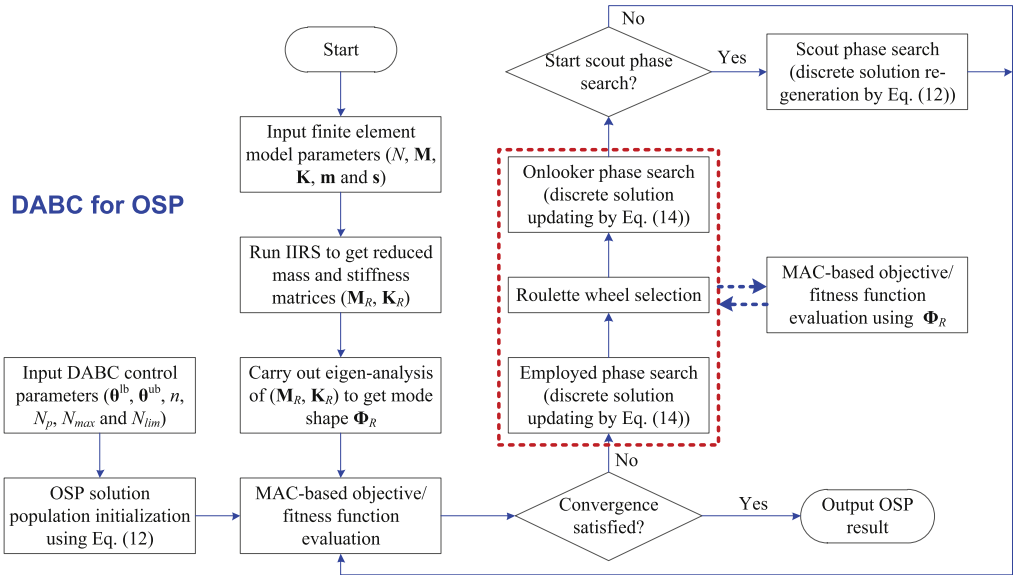

Figure 1. Flow chart of the proposed OSP algorithm using DABC.

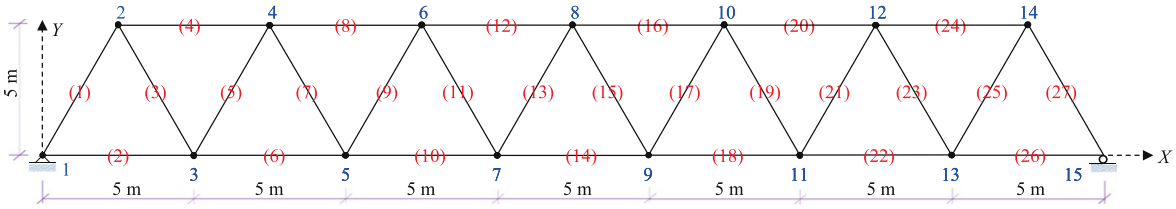

Figure 2. A 27 bar simply-supported truss bridge.

4. Numerical examples

To demonstrate the effectiveness and efficiency of the proposed OSP algorithm, we study three numerical examples to determine the sensor layout on a 27 bar truss bridge, a 21-storey building at the MIT campus and the 610 m high Canton Tower, respectively. In each example, two objective functions as given in equations (8) and (9) are studied, respectively. Because the proposed DABC algorithm is stochastic in nature, each run typically brings different solution. To avoid solution uncertainty, each optimization problem of OSP is repeated 50 times in the statistical simulations. The best solution with the minimum objective function value is taken as the representative OSP result. Nevertheless, the statistical convergence of 50 runs are also reported. The DABC parameter settings used in the simulations are given as follows: $N_{\mathrm{p}} = 50$, $N_{\mathrm{lim}} = 100$, $N_{\mathrm{max}} = 3000$, and $n =$ the given number of sensors. The numerical analyses are programmed in MATLAB® (The MathWorks, Inc., MA, USA) on a standard Intel (R) Core (TM) i7-4930 K 3.40 GHz PC with 32G RAM.

4.1. A 27 bar truss bridge

The performance of the proposed OSP scheme is first studied on a 27 bar truss bridge as shown in figure 2. The truss bridge is a simply supported structure with 27 bars and 15 nodes (e.g., the geometry, dimensions, as well as numbering system are illustrated in figure 2). The material and geometric properties of the truss elements are: Young's modulus $E = 200$ GPa, mass density $\rho = 7860$ kg m^{-3}, cross-sectional area of 0.01 m^2 for the elements numbered {1, 2, 4, 6, 8, 10, 12, 14, 16, 18, 20, 22, 24, 26, 27} and 0.005 m^2 for the elements numbered {3, 5, 7, 9, 11, 13, 15, 17, 19, 21, 23, 25} [41]. The natural periods of the first two modes become 0.127 and 0.051 s.

We study the OSP of eight sensors on the truss bridge. The truss bridge has 27 active DOFs in total for OSP (e.g., $m = 27$). The first six modes are used for the objective function calculation. The best optimal objective function values among 50 DABC runs and the corresponding OSP configurations are listed in table 1. It can be observed that the sensor layouts are slightly different if the objective function formulations are different (e.g., equation (8) versus equation (9)). The identical sensor locations based on equation (8) versus equation (9) are shaded with gray color. It is noted that, when a small number of sensors are given, most of the optimal sensor locations remain the same using different objective functions (see table 1). The two objective functions values are all less than 1×10^{-3}, which illustrates that the MAC off-diagonal values are extremely small. Thus, the OSP configurations ensure the smallest cross-correlation between two modes and make the modes most distinguishable between each other.

The convergence results for OSP of a 27 bar truss bridge are shown in figure 3. The worst, mean and best convergence

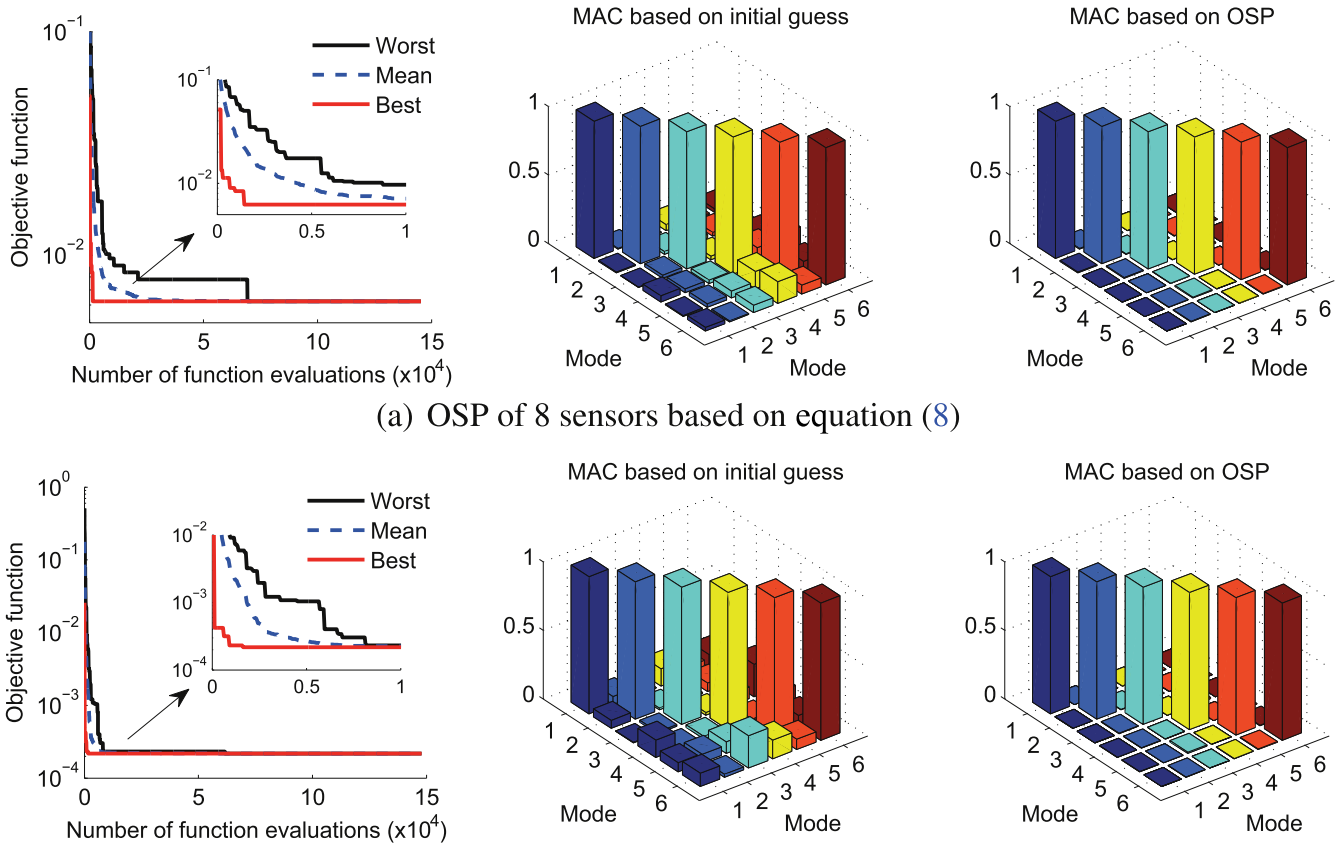

(a) OSP of 8 sensors based on equation (8)

(b) OSP of 8 sensors based on equation (9)

Figure 3. Convergence for OSP of a 27 bar truss bridge. Note that the best solution is listed as the representative OSP result (e.g., employed to calculate the MAC).

Table 1. OSP of a 27 bar truss bridge using eight sensors.

OSP based on equation (8)	$f_1(\boldsymbol{\vartheta})$	2.178×10^{-4}							
	Direction	x				y			
	Sensor number	1	2	3	4	5	6	7	8
	Node number	2	6	11	13	4	7	10	13
OSP based on equation (9)	$f_2(\boldsymbol{\vartheta})$	8.245×10^{-5}							
	Direction	x				y			
	Sensor number	1	2	3	4	5	6	7	8
	Node number	2	6	12	13	4	7	10	13

lines of the two different objective functions are given in figure 3, which are obtained from 50 DABC runs. It can be seen that the best solution converges quite fast, only after a small number of function evaluations (e.g., 2000), accounting for a high convergence efficiency of the proposed DABC algorithm. The MAC values obtained by the proposed OSP algorithm are also shown in figure 3, which are calculated based on the the best optimization solution. Again, small MAC off-diagonal values (e.g., close to zero) are observed through those figures. Note that the CPU time for each DABC run in this example is close to 20 s.

4.2. A 21-storey building at the MIT campus

In this second example, we test the proposed algorithm on OSP of a 21-storey building, called the Green Building, at the MIT campus in Cambridge, Massachusetts, as illustrated in figure 4(a). The Green Building is currently the tallest building in Cambridge with 21 stories. The building was designed by Pei and constructed during the period of 1962–1964. The Green Building is 83.7 m tall with a footprint of 16.5 m by 34 m. The short and long directions of the Green Building are represented by East–West and North–South

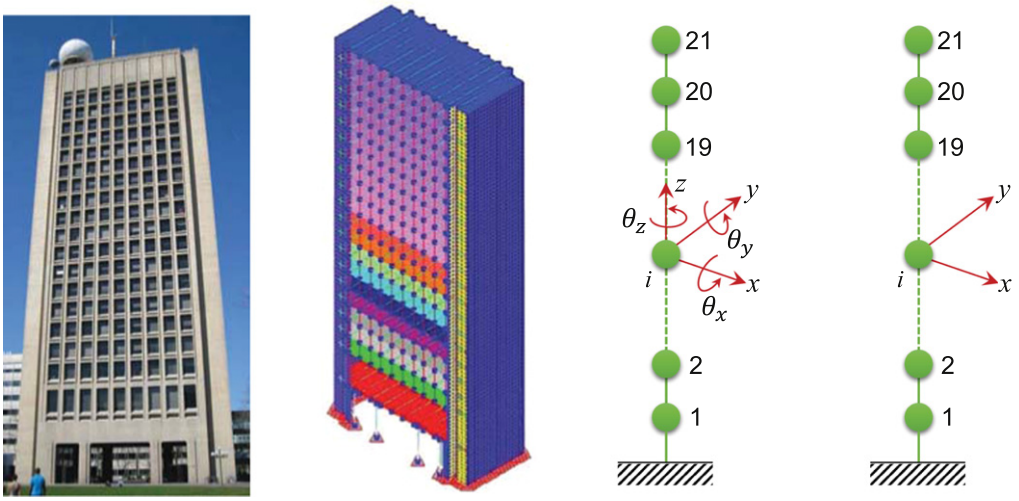

(a) Green Building (b) Full scale model (c) 126 DOFs (d) 42 DOFs

Figure 4. A 21-storey building (Green Building) at the MIT campus and its FE models.

directions corresponding to *x*- and *y*-axes, respectively. Other information of this building can be found in [42, 43].

Before conducting OSP of the Green Building, we develop a full scale FE model of the building with beam and shell elements, as shown in figure 4(b), using Autodesk Simulation Multiphysics (Autodesk, Inc., CA, US). Then a 3D simplified lumped-mass beam model is obtained based on the full scale model through static condensation given in figure 4(c). Each floor of the simplified model has a point mass with six DOFs (e.g., three translational and three rotational). Therefore, the total number of DOFs of the simplified beam model is 126. The detailed process of FE modeling and static condensation of this building is described in [42]. Note that the first two periods of the Green Building, obtained from the FE model, are 1.473 and 1.328 s.

In application of the proposed algorithm to OSP of the Green Building, we only consider the horizontally translational DOFs since the responses of torsional DOFs are difficult to measure in real applications. Nevertheless, additional sensors could be placed based on the optimal sensor layout for translational DOFs and thus gain insights into the torsional behavior of the building. In this study, we exclude the torsional as well as the vertical DOFs of the simplified beam model in the OSP process. Therefore, we first apply the IIRS technique described in section 2.1 to the simplified beam model and obtain a reduced model consisting of horizontally translational DOFs only, as shown in figure 4(d). Note that the frequencies of the reduced model from IIRS are identical to those of the simplified beam model. The reduced model has 42 DOFs which are used for OSP.

We study the OSP of 12 sensors on the Green Building. The first ten modes of the reduced model are used in calculating the MAC values in the objective function. The optimal objective function values and the OSP configurations for the Green Building are summarized in table 2. It can be observed that big discrepancies between the two OSP configurations exist. For example, only two sensor locations are identical along the *x*-direction while the sensor locations are completely different along the *y*-direction. This illustrates that the OSP configuration strongly depends on the objective function used in the optimization process. If two or multiple objective functions are used for OSP, compromises have to be made. This phenomenon was also observed by Yi *et al* [25].

The convergence results for OSP of the Green Building are given in figure 5, in which the worst, mean and best convergence lines of the two different objective functions are plotted. It can be seen that the objective function $f_2(\boldsymbol{\vartheta})$ (equation (9)) converges much faster compared with $f_1(\boldsymbol{\vartheta})$ (equation (8)). It appears to be easier to find the optimum when equation (9) is used as the objective function. In addition, the deviation of the convergence lines for $f_2(\boldsymbol{\vartheta})$ is smaller than that of $f_1(\boldsymbol{\vartheta})$, accounting for a much more robust convergency when Equation (9) is used for OSP. The MAC values are also shown in figure 5, calculated based on the the representative solution. In general, the MAC off-diagonal values remain small for both cases. Compared figures 5(a) and (b), it is observed that the maximum MAC off-diagonal value based on the optimization of $f_2(\boldsymbol{\vartheta})$ is slightly larger than that based on $f_1(\boldsymbol{\vartheta})$. This is reasonable since $f_2(\boldsymbol{\vartheta})$ is formulated using least squares. It is possible that one least square is relatively large while keeping other least squares small, leading to the smallest summation of the least squares. The CPU time of each DABC run is about 45 s.

4.3. Canton Tower

In the third example, we test the performance of proposed OSP algorithm on the Canton Tower with a total height of 610 m (see figure 6(a)), which was previously studied by Yi *et al* [19, 25, 26]. The proposed OSP algorithm in this paper is compared with the IMA presented in [26]. The Canton Tower comprises two parts including a 454 m high main tower and a 156 m high steel antenna mast. The main tower consists of a reinforced concrete interior tube and a steel lattice courter

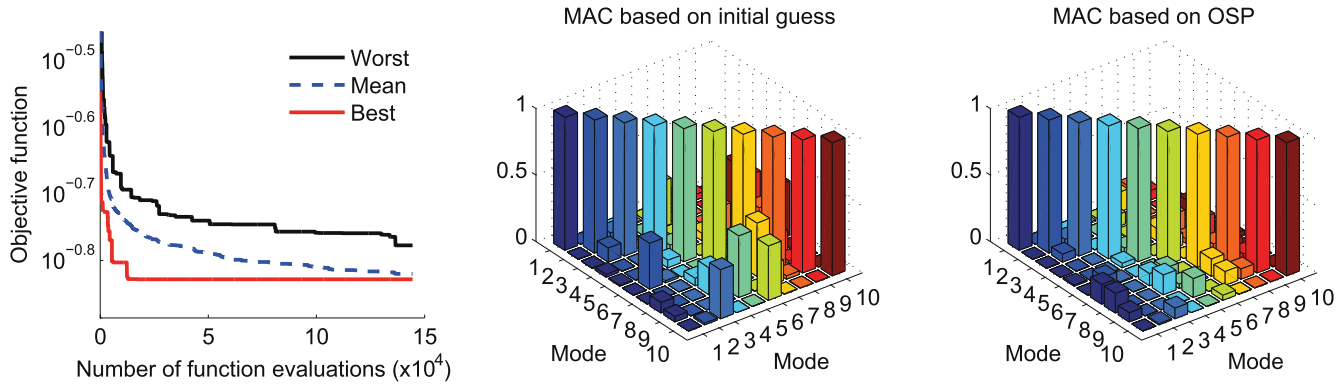

(a) OSP of 12 sensors based on equation (8)

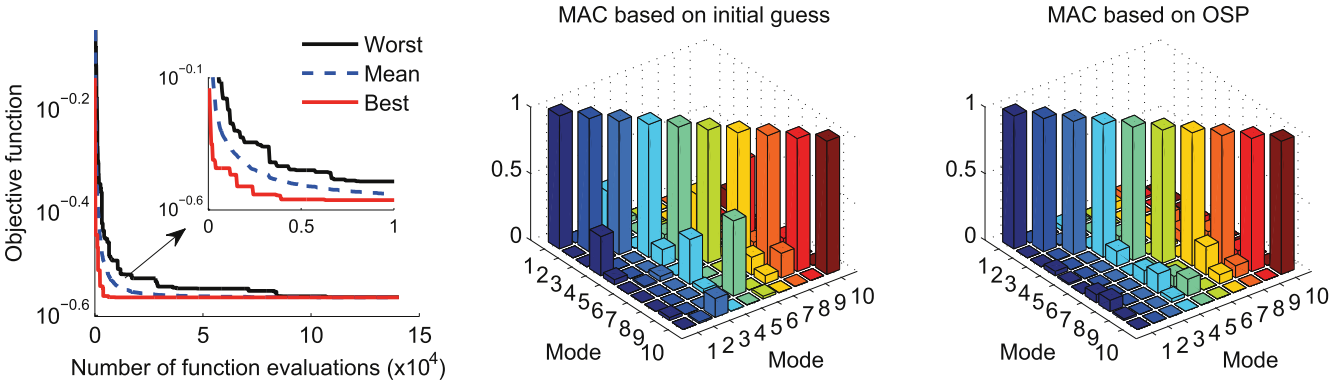

(b) OSP of 12 sensors based on equation (9)

Figure 5. Convergence for OSP of a 21-storey building (Green Building) at the MIT campus. Note that the best solution is listed as the representative OSP result (e.g., employed to calculate the MAC).

Table 2. OSP of a 21-storey building at the MIT campus using 12 sensors.

OSP based on equation (8)	$f_1(\vartheta)$	0.1486										
	Direction	x								y		
	Sensor number	1	2	3	4	5	6	7	8	9	10	11	12
	Floor number	2	6	7	12	15	16	17	20	1	7	15	20
OSP based on equation (9)	$f_2(\vartheta)$	0.2722										
	Direction	x								y		
	Sensor number	1	2	3	4	5	6	7	8	9	10	11	12
	Floor number	1	4	5	9	10	15	16	19	2	8	14	19

structure. Other descriptions of this structure can be found in [44].

Similar to the previous example, in order to provide input data of the tower to the proposed OSP algorithm, a FE model is first required. As shown in figure 6(b), the full scale FE model developed by Ni *et al* [44] using ANSYS (ANSYS, Inc., PA, USA) is used, which consists of 122 476 beam and shell elements, 86 370 nodes and 505 164 DOFs. To apply the proposed OSP algorithm to the Canton Tower, a simplified 3D beam model with lumped mass established by Ni *et al* [44] is employed, as illustrated in figure 6(c). The simplified model consists of 37 beam elements, with 27 elements for the main tower and ten elements for the antenna mast. Each beam node has five DOFs (e.g, two horizontally translational and three torsional) neglecting the vertical DOF. Therefore, the beam model has 185 DOFs in total as shown in figure 6(c). For the process of condensing the full scale model to the simplified beam model, the readers are referred to [44]. Similar to the previous example, we only consider the horizontally translational DOFs for OSP. Therefore, we first reduced the 3D beam model using the IIRS technique described in section 2.1 and obtain a reduced model only

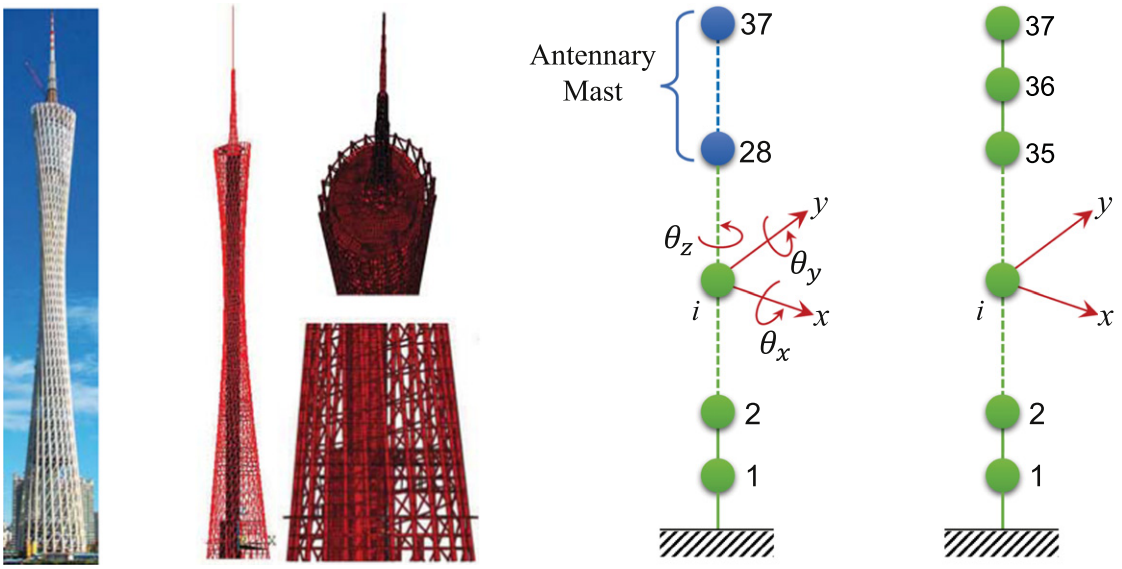

(a) Canton Tower (b) Full scale model (c) 185 DOFs (d) 74 DOFs

Figure 6. Canton Tower and its FE models [44]. Copyright 2012 by Techno-Press.

Table 3. OSP of the Canton Tower using 20 sensors.

Reference [26]	$f_1(\vartheta)$	0.5394										
	Direction	x					y					
	Sensor number	1	2	3	4	5	10	11	12	13	14	15
	Floor number	2	6	14	20	21	1	2	4	5	6	7
	Sensor number	6	7	8	9	—	16	17	18	19	20	—
	Floor number	22	23	24	29	—	11	16	20	22	23	—
OSP based on equation (8)	$f_1(\vartheta)$	0.4816										
	Direction	x					y					
	Sensor number	1	2	3	4	5	10	11	12	13	14	15
	Floor number	2	3	17	18	19	21	2	3	10	17	19
	Sensor number	6	7	8	9	—	16	17	18	19	20	—
	Floor number	20	21	22	23	—	20	21	22	24	28	—
OSP based on equation (9)	$f_2(\vartheta)$	2.1766										
	Direction	x						y				
	Sensor number	1	2	3	4	5	6	12	13	14	15	16
	Floor number	1	2	3	4	5	14	3	4	5	8	17
	Sensor number	7	8	9	10	11	—	17	18	19	20	—
	Floor number	18	19	20	21	26	—	19	20	23	27	—

taking into account horizontally translational DOFs, as shown in figure 6(d). The reduced model has a total number of 74 DOFs which are considered as the candidate sensor locations. Note that the same reduced model was used for OSP in [19, 25, 26].

Table 3 summarizes the OSP results of the Canton Tower with 20 sensors. Again, it is observed that the sensor locations have discrepancies if the objective function used for OSP is different (e.g., $f_1(\vartheta)$ or $f_2(\vartheta)$). For example, only ten sensor locations are identical as shown in table 3. The number of sensors in the x (or y) direction also changes along with the form of the objective function. The same conclusion is obtained herein as mentioned in the previous example: the OSP configuration strongly depends on the objective function formulation.

The OSP result obtained by the proposed algorithm is also compared with the one obtained by the IMA presented in

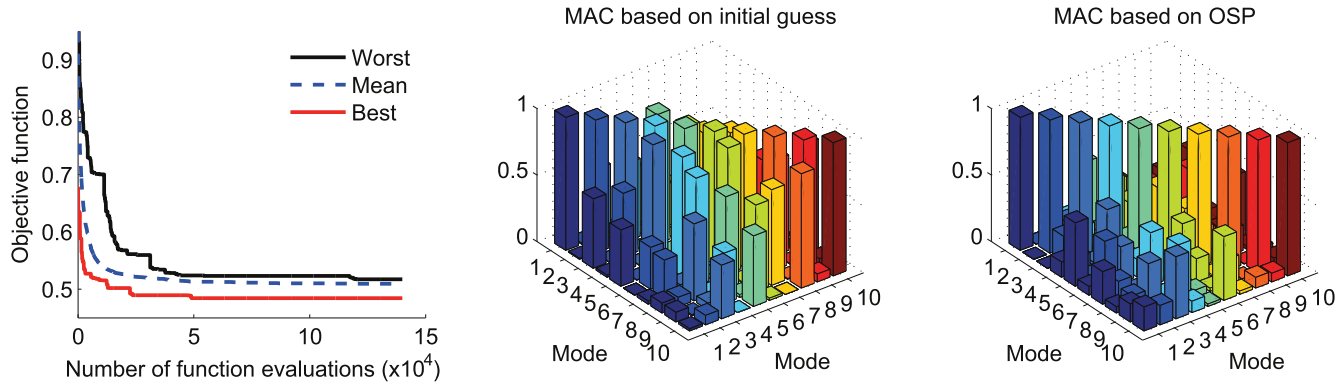

(a) OSP of 20 sensors based on equation (8)

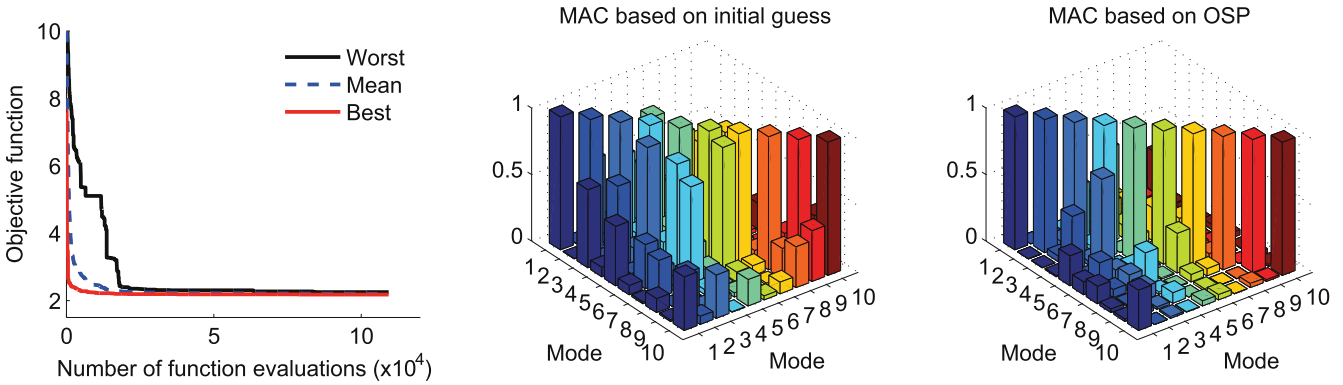

(b) OSP of 20 sensors based on equation (9)

Figure 7. Convergence for OSP of the 610 m high Canton Tower. Note that the best solution is listed as the representative OSP result (e.g., employed to calculate the MAC).

[26]. It is noted that the IMA has a dual encoding mechanism, which transforms the discrete OSP problem into a continuous optimization problem. The constraints can be handled via solution regeneration in the IMA, which is different from the penalty strategy proposed in this paper. In the comparison, the maximum MAC off-diagonal value is used to formulate the objective (see equation (8)). It is seen from table 3 that the objective function value (0.4816) obtained by the proposed algorithm is smaller than the one (0.5394) obtained by the IMA. This indicates that the proposed OSP algorithm finds a better optimal solution compared with the one from the IMA. By comparing the objective function value, we may conclude that the proposed OSP algorithm performs better than the IMA which has been proved to be an effective OSP approach [26].

Figure 7 depicts the convergence for OSP of the Canton Tower using different objective functions. Statistical convergence lines (e.g., best, mean and worst) of the objective functions are reported. It can be seen that, in general, the objective functions converge quickly. Again, a better convergency (e.g., more efficient and more robust) is observed for the case when the summation of least squares of the MAC off-diagonal values is used as the objective function. The MAC values are also shown in figure 7. It can be seen that the maximum MAC off-diagonal value based on OSP in figure 7(b) is slightly larger than the one in figure 7(a); however, the rest MAC off-diagonal values are overall smaller in figure 7(b). In general, the summation of least squares of the MAC off-diagonal values (e.g., $f_2(\boldsymbol{\vartheta})$ in equation (9)) appears to be a better option for the OSP objective function formulation. Noteworthy, the CPU time of each DABC run for OSP of the Canton Tower is about 47 s.

5. Experimental validation

In order to validate the OSP performance in SHM, we study a three-story two-bay steel frame in the MIT structural laboratory, as shown in figure 8(a). The structure consists of 39 frame elements and 24 nodes with the bottom nodes fixed at the base. The elements are bolted together to form the spatial frame structure. Each element of the steel frame has the dimension of 5.08 × 0.635 × 60.96 cm. The steel material properties are given as follows: Young's modulus $E = 196$ GPa, Poisson's ratio 0.26 and mass density $\rho = 7880$ kg m^{-3}. A full scale FE model is built for OSP as illustrated in figure 8(b). The model has a total number of 108 DOFs. Nevertheless, only the 36 translational DOFs (along the x- and y-directions) are considered for OSP. The first seven modes computed using the FE model as shown in figure 9 are employed in the process of OSP. It is noted that the modal analysis results show that the structural stiffness

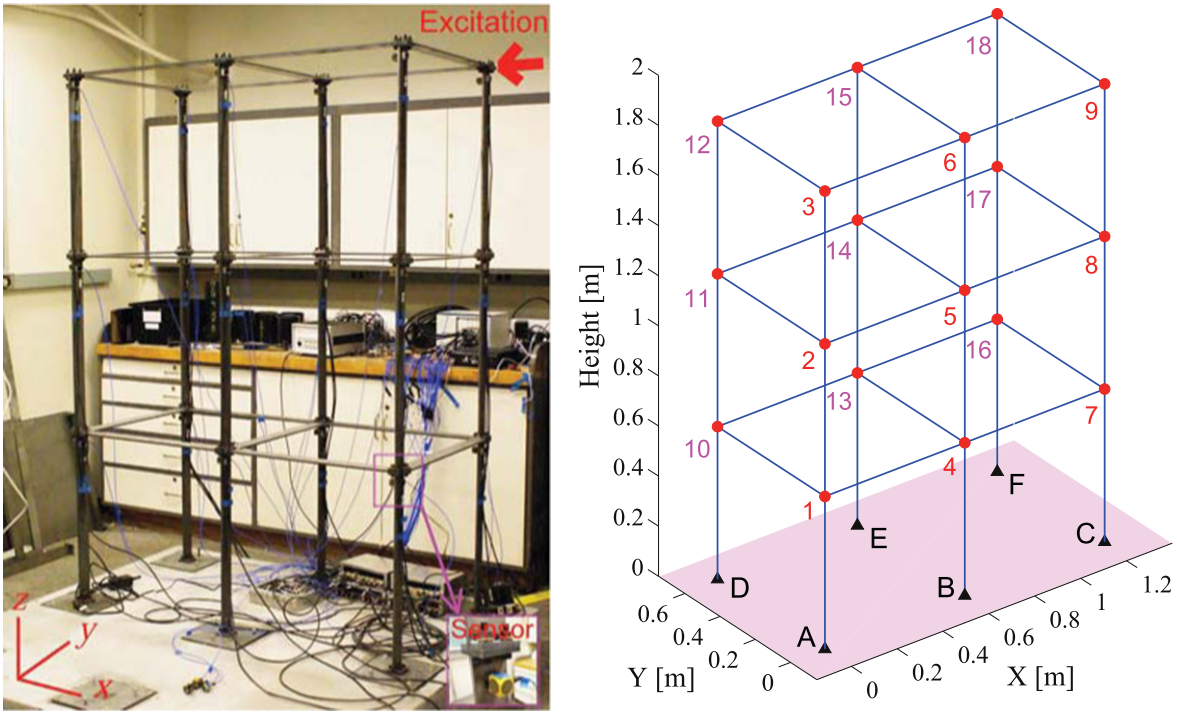

(a) Experimental structure (spatial frame) (b) Finite element model

Figure 8. A three-storey two-bay experimental frame structure in the MIT structural lab.

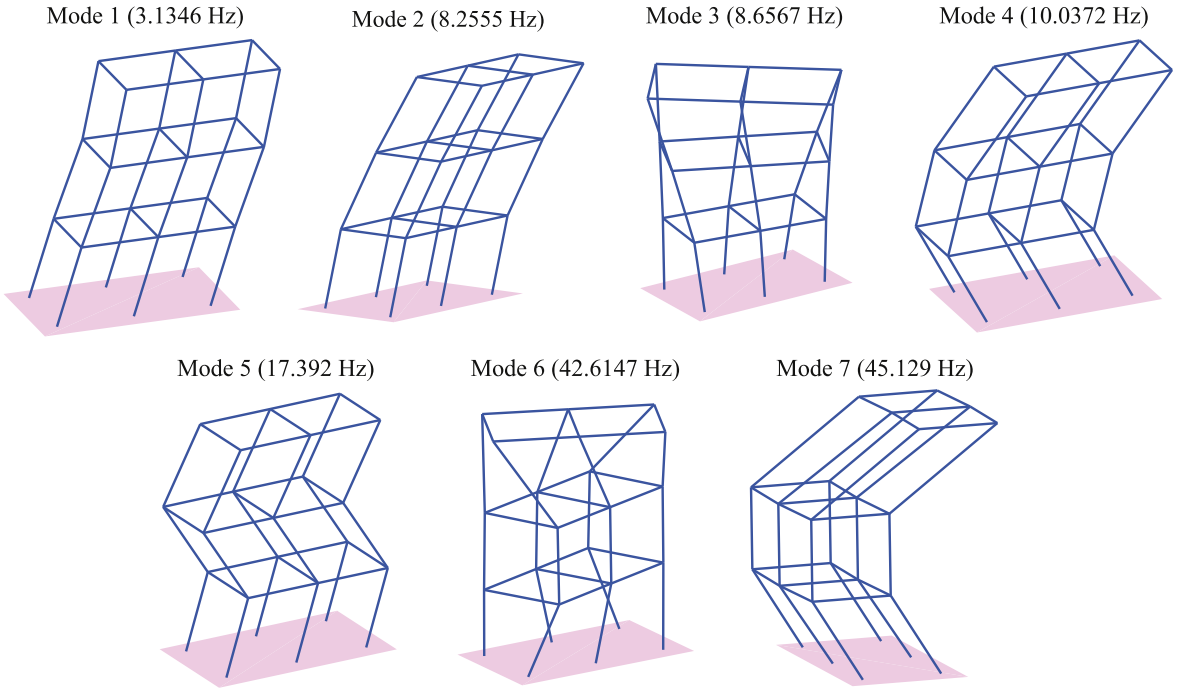

Figure 9. The first seven modes of the frame structure computed by the finite element model.

along the x-direction is significantly larger than that along the y-direction.

The structure is instrumented with 18 triaxial piezoelectric accelerometers which are attached close to the 18 active nodes. A shaker mounted at node #18 is used to excite the structure along the x-direction (e.g., the flexible direction) as shown in figure 8(a). The excitation in this test is a Gaussian white noise sequence. The sampling rate of data acquisition is 6 kHz and 22 s long data were recorded for analysis. We downsample the data to 1 kHz and employ it in

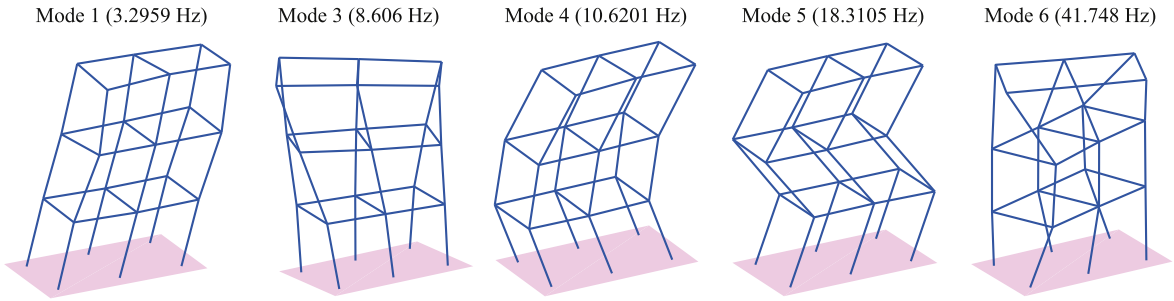

Figure 10. The identified five modes of the frame structure using experimental data.

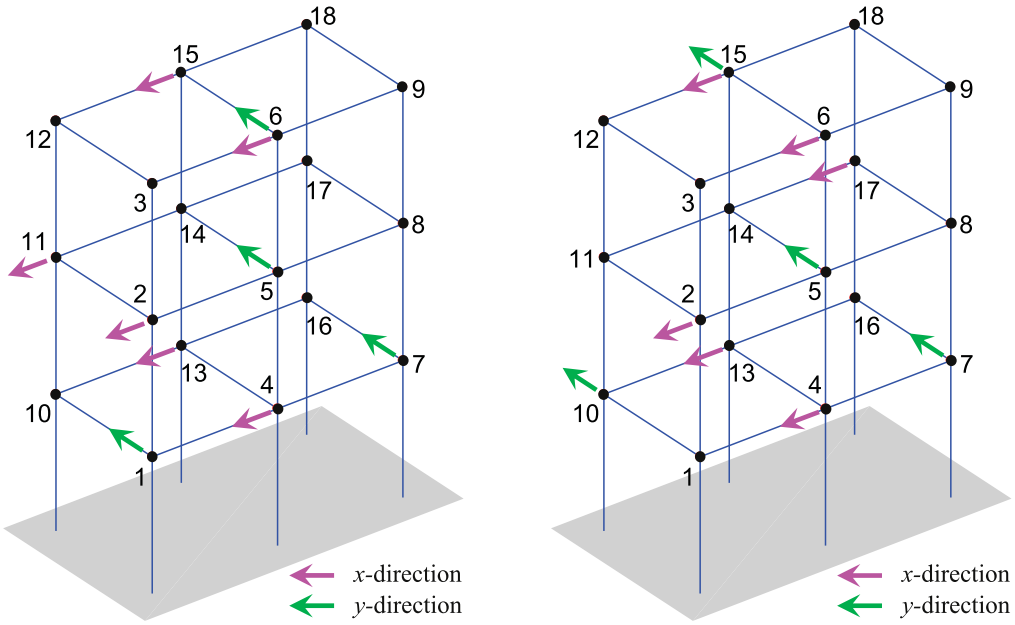

(a) OSP based on Equation (8) (b) OSP based on Equation (9)

Figure 11. Optimal layout of ten sensors for the experimental frame structure.

all the analyses in this validation example. The modal properties of the structure are first identified using the frequency domain decomposition (FDD) [45] based on all the nodal measurements. Five modes (e.g., frequencies and mode shapes) are identified and presented in figure 10. It is noteworthy to mention that the second mode is missing in the identified modal properties. This is because that the second mode along the y-direction is not well excited in the experiment (e.g., the excitation is along the x-direction) and it has a quite minor peak in the singular value plot of the power spectral density (PSD) matrix [46]. The identified modes herein are then used as reference quantities to compute MAC for the validation of the proposed OSP algorithm.

Similar to the numerical examples discussed in section 4, we carry out the OSP of 10 accelerometers for the experimental frame structure based on $f_1(\boldsymbol{\vartheta})$ (see equation (8)) and $f_2(\boldsymbol{\vartheta})$ (see equation (9)), respectively. The optimal sensor layouts for both cases are visualized in figure 11. It can be seen that most of the sensor locations (e.g., 7 out of 10) between the two cases are identical. The discrepancy is mainly present in the sensor layout along the y-direction. It is interesting that since the structure has symmetric characteristics, both sensor layouts in figure 11 are theoretically identical for modal identification along both x- and y-directions, because the nodes can be symmetrically presented in pairs. For example, node #11 corresponds to #17 along the x-direction, nodes #1 and #6 correspond to #10 and #15, respectively, along the y-direction. It appears that the spatial sensor layout in figure 11(b) might be better to capture structural torsional characteristics compared to the one shown in figure 11(a).

Figure 12 shows the MAC plots of five modes with respect to different sensor layouts. Note that the MAC values herein are computed following the procedure: (i) select the measurements corresponding to the sensing DOFs (a limited number of sensor locations) from the recorded complete acceleration responses; (ii) apply FDD to identify the modal properties using the selected measurements; (iii) compute the MAC values based on the identified mode shapes in the previous step and the reference mode shapes (see figure 10)

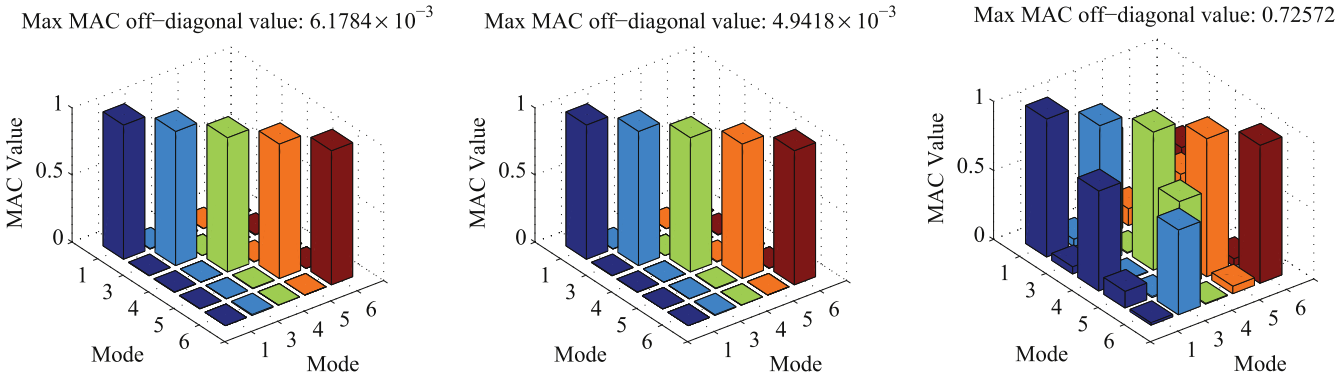

Figure 12. MAC of the identified modes for the experimental frame structure based on both OSP and arbitrary sensor layout.

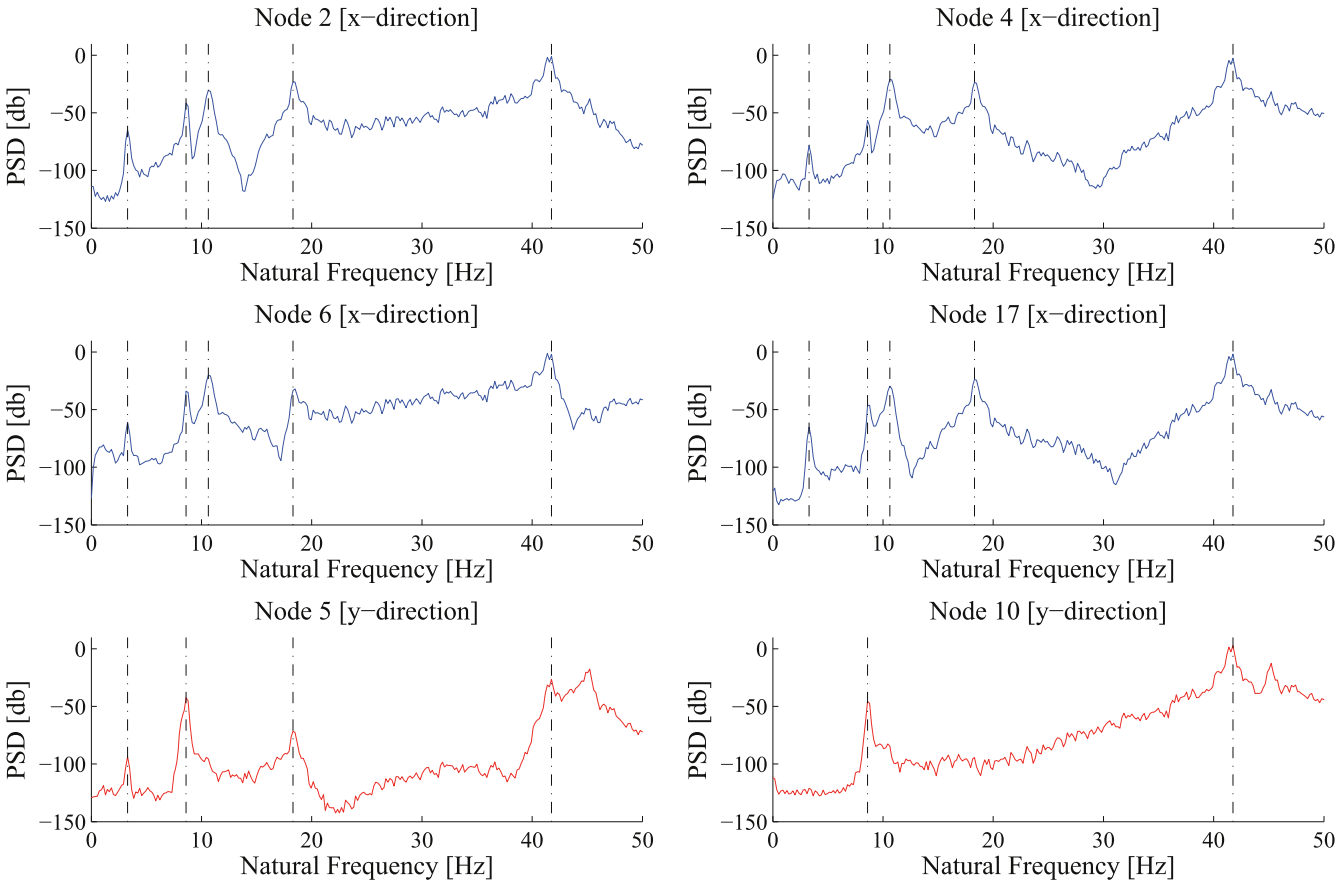

Figure 13. Experimental frequency responses of some typical OSP nodes.

identified from complete measurements. Note that an arbitrary set of nodes are selected as the sensor layout for comparison with the OSP results: nodes #1, #4, #8, #10, #13, #16 for *x*-direction sensing and nodes #1, #2, #4, #10 for *y*-direction sensing. It can be seen from figure 12 that the maximum MAC off-diagonal value based on OSP is quite small (e.g., close to zero), while in the arbitrary sensor layout case, the MAC off-diagonal values are in general quite large with the maximum value of 0.7257. The results given in figure 12 demonstrate the effectiveness of the proposed OSP algorithm.

In addition, figure 13 shows the acceleration PSDs at six typical nodes based on OSP. This figure spans a frequency range from 0 to 50 Hz, which covers the first few modes of the experimental frame structure. It can be seen that the modes along the *x*-direction as well as the torsional modes are well excited. Distinctive peaks can be observed, which illustrates that rich structural information is included in the measurements at sensor locations based on OSP. Since the *y*-direction modes are not well excited, the sensors along this direction mainly contribute to measure structural torsional characteristics.

```
Input finite element model parameters: number of DOFs N, mass matrix M, stiffness matrix K, master
                                       DOFs m, and slave DOFs s.
Run model reduction: call IIRS(N,M,K,m,s) to calculate the reduced mass/stiffness matrices M_R and K_R.
Calculate mode shapes of the reduced model: Φ_R.

Input DABC parameters: θ^lb, θ^ub, n, N_p, N_max and N_lim.
Initialization:
For k = 1 to N_p
  For i = 1 to n
    Θ(k,i) = θ^lb(i) + round(rand[0,1]*(θ^ub(i) - θ^lb(i)))    //initialize the population
  End For
End For
MAC-based objective function solver: Call ObjMAC(Θ,Φ_R) to compute the fitness function fit(Θ).
Sort the population Θ based on fit(Θ) and eliminate the worst N_p/2 of them.
Set limit = 0;                                //counters to record non-updated trials
Set iter = 0;

Optimization:
While (iter ≤ N_max)

  For k = 1 to N_p/2                          //employed phase searching
    Set β = Θ(k,:);                           //select the kth solution for updating
    i = fix(rand[0,1]*n) + 1;                 //select the ith parameter for updating
    While (j = k)                             //select the jth neighborhood solution
      j = fix(rand[0,1]* N_p/2) + 1;
    End While
    b = find(fit(Θ) = min(fit(Θ)));           //find the current best solution in the population
    //create employed candidate solution
    β(i) = Θ(k,i) + round(rand[-1,1]*(Θ(k,i) - Θ(j,i)) + rand[0,1]*(Θ(b,i) - Θ(k,i)));
    MAC-based objective function solver: Call ObjMAC(β,Φ_R) to compute fit(β).
    If fit(β) > fit(Θ(k,:))                   //compare the old and the new solutions
      Θ(k,:) = β;                             //replace the old solution by the new one
      fit(Θ(k,:)) = fit(β);
      limit(k) = 0;
    Else
      limit(k) = limit(k) + 1;
    End If
  End For

  For i = 1 to N_p/2                          //compute associated solution probability
    p(i) = fit(θ(i,:))/sum(fit(θ));
  End For

  For k = 1 to N_p/2                          //onlooker phase searching
    If rand[0,1] < p(k)
      Set β = Θ(k,:);                         //select the kth solution for updating
      i = fix(rand[0,1]*n) + 1;               //select the ith parameter for updating
      While (j = k)                           //select the jth neighborhood solution
        j = fix(rand[0,1]* N_p/2) + 1;
      End While
      b = find(fit(Θ) = min(fit(Θ)));         //find the current best solution in the population
      //create onlooker candidate solution
      β(i) = Θ(k,i) + round(rand[-1,1]*(Θ(k,i) - Θ(j,i)) + rand[0,1]*(Θ(b,i) - Θ(k,i)));
      MAC-based objective function solver: Call ObjMAC(β,Φ_R) to compute fit(β).
      If fit(β) > fit(Θ(k,:))                 //compare the old and the new solutions
        Θ(k,:) = β;                           //replace the old solution by the new one
        fit(Θ(k,:)) = fit(β);
        limit(k) = 0;
      Else
        limit(k) = limit(k) + 1;
      End If
    End If
  End For

  For k = 1 to N_p/2                          //scout phase searching
    If limit(k) > N_lim
      For i = 1 to n
        Θ(k,i) = θ^lb(i) + round(rand[0,1]*(θ^ub(i) - θ^lb(i)))  //create scout solution
      End For
      MAC-based objective function solver: Call ObjMAC(Θ(k,:),Φ_R) to compute fit(Θ(k,:)).
      limit(i) = 0;
    End If
  End For

  Ind = find(fit(Θ) = min(fit(Θ)));           //find the index of the best solution
  θ_best = Θ(Ind,:);                          //record the best solution

  iter = iter + 1;

End While
```

Figure A1. Pseudo code of the proposed OSP algorithm using DABC. Note that the programming code of the proposed algorithm can be released upon request.

6. Conclusions

In this work, we investigate the OSP problem in SHM. The general objective of this study is to propose an intelligent approach to determine the optimal sensor layout on a structure, that provides the maximum dynamic information of this structure, given a limited number of sensors. The OSP problem is first formulated as a discrete (integer) optimization problem with constraints, where the integer variables denote the possible sensor locations. The objective function for the optimization problems is defined in terms of the MAC values calculated from the selected mode shapes of a reduced model. The constraints are basically determined by the equality condition of the total number of given sensors as well as the parameter bounds. The equality constraint is handled by a penalty strategy in the optimization process. A discrete optimization algorithm called DABC is proposed to solve the OSP problem. The optimal sensor layout can be determined as long as the DABC finds the optimizer of the objective function.

Three numerical examples (including a truss bridge and two high-rise buildings) are investigated to test the applicability of the proposed DABC algorithm to OSP. Numerical results show that the proposed method is efficient and effective in OSP of structural systems based on modal characteristics. Nevertheless, it is noted from the numerical results that the OSP configuration depends on the objective function formulation used in the optimization process. The objective function based on the summation of least squares of the MAC off-diagonal values has a faster and more robust convergency compared to the case when the maximum MAC off-diagonal value is used. Furthermore, we validate the proposed OSP algorithm using a laboratory experimental frame structure. Again, results show the algorithm's effectiveness. Future studies would focus on field SHM applications and damage detection based on the sensor layout obtained by the proposed OSP algorithm.

Acknowledgments

The authors would like to acknowledge the support provided by Royal Dutch Shell through the MIT Energy Initiative. We thank Professor Ting-Hua Yi from Dalian University of Technology for his discussions in the numerical case studies. Thanks are also due to Justin Chen, Reza Mohammadi Ghazi and James Long for their efforts on collecting the experimental data.

Appendix A. Pseudo code of the proposed OSP algorithm

The pseudo code of the proposed OSP algorithm is given in figure A1.

References

[1] Sun H 2014 Development of hierarchical optimization-based models for multiscale damage detection *PhD Thesis* Columbia University, New York
[2] Yuen K-V, Beck J L and Au S K 2004 Structural damage detection and assessment by adaptive Markov Chain Monte Carlo simulation *Struct. Control Health Monit.* **11** 327–47
[3] Perry M J, Koh C G and Choo Y S 2006 Modified genetic algorithm strategy for structural identification *Comput. Struct.* **84** 529–40
[4] Jiang X, Mahadevan S and Adeli H 2007 Bayesian wavelet packet denoising for structural system identification *Struct. Control Health Monit.* **14** 333–56
[5] Nayeri R D, Masri S F, Ghanem R G and Nigbor R L 2008 A novel approach for the structural identification and monitoring of a full-scale 17-story building based on ambient vibration measurements *Smart Mater. Struct.* **17** 025006
[6] Yuen K-V 2012 Updating large models for mechanical systems using incomplete modal measurement *Mech. Syst. Signal Process.* **28** 297–308 (Interdisciplinary and Integration Aspects in Structural Health Monitoring)
[7] Sun H, Luş H and Betti R 2013 Identification of structural models using a modified artificial bee colony algorithm *Comput. Struct.* **116** 59–74
[8] Bao C, Hao H and Li Z-X 2013 Multi-stage identification scheme for detecting damage in structures under ambient excitations *Smart Mater. Struct.* **22** 045006
[9] Yuen K-V and Katafygiotis L S 2014 Modal decomposition using multi-channel response measurements *Probabilistic Eng. Mech.* **37** 60–73
[10] Sun H, Waisman H and Betti R 2014 A multiscale flaw detection algorithm based on XFEM *Int. J. Numer. Methods Eng.* **100** 477–503
[11] Mukhopadhyay S, Luş H and Betti R 2015 Structural identification with incomplete instrumentation and global identifiability requirements under base excitation *Struct. Control Health Monit.* **22** 1024–47
[12] Chen J G, Wadhwa N, Cha Y-J, Durand F, Freeman W T and Buyukozturk O 2015 Modal identification of simple structures with high-speed video using motion magnification *J. Sound Vib.* **345** 58–71
[13] Cha Y-J and Buyukozturk O 2015 Structural damage detection using modal strain energy and hybrid multiobjective optimization *Comput.-Aided Civ. Infrastruct. Eng.* **30** 347–58
[14] Kammer D C 1991 Sensor placement for on-orbit modal identification and correlation of large space structures *J. Guid. Control Dyn.* **14** 251–9
[15] worden K and burrows A P 2001 optimal sensor placement for fault detection *Eng. Struct.* **23** 885–901
[16] Papadimitriou C 2004 Optimal sensor placement methodology for parametric identification of structural systems *J. Sound Vib.* **278** 923–47
[17] Papadimitriou C and Lombaert G 2012 The effect of prediction error correlation on optimal sensor placement in structural dynamics *Mech. Syst. Signal Process.* **28** 105–27
[18] Rao A R M and Anandakumar G 2007 Optimal placement of sensors for structural system identification and health monitoring using a hybrid swarm intelligence technique *Smart Mater. Struct.* **16** 2658
[19] Yi T-H, Li H-N and Gu M 2011 Optimal sensor placement for structural health monitoring based on multiple optimization strategies *Struct. Des. Tall Spec. Build.* **20** 881–900
[20] Flynn E B and Todd M D 2010 A bayesian approach to optimal sensor placement for structural health monitoring with application to active sensing *Mech. Syst. Signal Process.* **24** 891–903

[21] Chang M and Pakzad S N 2015 Optimal sensor configuration for flexible structures with multi-dimensional mode shapes *Smart Mater. Struct.* **24** 055012
[22] Yao L, Sethares W A and Kammer D C 1993 Sensor placement for on-orbit modal identification via a genetic algorithm *AIAA J.* **31** 1922–8
[23] Guo H Y, Zhang L, Zhang L L and Zhou J X 2004 Optimal placement of sensors for structural health monitoring using improved genetic algorithms *Smart Mater. Struct.* **13** 528–34
[24] Lian J, He L, Ma B, Li H and Peng W 2013 Optimal sensor placement for large structures using the nearest neighbour index and a hybrid swarm intelligence algorithm *Smart Mater. Struct.* **22** 095015
[25] Yi T-H, Li H-N and Zhang X-D 2012 Sensor placement on canton tower for health monitoring using asynchronous-climb monkey algorithm *Smart Mater. Struct.* **21** 125023
[26] Yi T-H, Li H-N and Zhang X-D 2015 Health monitoring sensor placement optimization for canton tower using immune monkey algorithm *Struct. Control Health Monit.* **22** 123–38
[27] Yi T-H, Li H-N, Song G and Zhang X-D 2015 Optimal sensor placement for health monitoring of high-rise structure using adaptive monkey algorithm *Struct. Control Health Monit.* **22** 667–81
[28] Yuen K-V, Katafygiotis L S, Papadimitriou N C and Mickleborough C 2001 Optimal sensor placement methodology for identification with unmeasured excitation *J. Dyn. Syst., Meas., Control* **123** 677–86
[29] Chow H M, Lam H F, Yin T and Au S K 2011 Optimal sensor configuration of a typical transmission tower for the purpose of structural model updating *Struct. Control Health Monit.* **18** 305–20
[30] Yuen K-V and Kuok S-C 2015 Efficient bayesian sensor placement algorithm for structural identification: a general approach for multi-type sensory systems *Earthq. Eng. Struct. Dyn.* **44** 757–74
[31] Cha Y-J, Agrawal A K, Kim Y and Raich A M 2012 Multi-objective genetic algorithms for cost-effective distributions of actuators and sensors in large structures *Expert Syst. Appl.* **39** 7822–33
[32] Cha Y-J, Raich A, Barroso L and Agrawal A 2013 Optimal placement of active control devices and sensors in frame structures using multi-objective genetic algorithms *Struct. Control Health Monit.* **20** 16–44
[33] Friswell M I, Garvey S D and Penny J E T 1995 Model reduction using dynamic and iterated IRS techniques *J. Sound Vib.* **186** 311–23
[34] Allemang R J and Brown D L 1982 A correlation coefficient for modal vector analysis *Proc. 1st Int. Modal Analysis Conf.* (*Kissimmee, FL, USA*) pp 110–116
[35] Karaboga D and Basturk B 2007 A powerful and efficient algorithm for numerical function optimization: artificial bee colony (abc) algorithm *J. Glob. Optim.* **39** 459–71
[36] Sun H, Waisman H and Betti R 2013 Nondestructive identification of multiple flaws using XFEM and a topologically adapting artificial bee colony algorithm *Int. J. Numer. Methods Eng.* **95** 871–900
[37] Sun H and Betti R 2014 Simultaneous identification of structural parameters and dynamic input with incomplete output-only measurements *Struct. Control Health Monit.* **21** 868–89
[38] Li B, Li Y and Gong L 2014 Protein secondary structure optimization using an improved artificial bee colony algorithm based on AB off-lattice model *Eng. Appl. Artif. Intell.* **27** 70–9
[39] Li B and Yao Y 2014 An edge-based optimization method for shape recognition using atomic potential function *Eng. Appl. Artif. Intell.* **35** 14–25
[40] Sun H and Betti R 2015 A hybrid optimization algorithm with Bayesian inference for probabilistic model updating *Comput.-Aided Civ. Infrastruct. Eng.* **30** 602–19
[41] Sun H and Büyüköztürk O 2015 Identification of traffic-induced excitations of truss bridges through heterogeneous data fusion *Smart Mater. Struct.* **24** 075032
[42] Trocha P A 2013 Characterization of structural properties and dynamic behavior using distributed accelerometer networks and numerical modeling *Master Thesis* Massachusetts Institute of Technology, Cambridge
[43] Çelebi M, Toksöz N and Büyüköztürk O 2014 Rocking behavior of an instrumented unique building on the mit campus identified from ambient shaking data *Earthq. Spectra* **30** 705–20
[44] Ni Y Q, Xia Y, Lin W, Chen W H and Ko J M 2012 SHM benchmark for high-rise structures: a reduced-order finite element model and field measurement data *Smart Struct. Syst.* **10** 411–26
[45] Brincker R, Zhang L and Andersen P 2001 Modal identification of output-only systems using frequency domain decomposition *Smart Mater. Struct.* **10** 441
[46] Mohammadi Ghazi R and Büyüköztürk O 2015 Damage detection with small data set using energy-based nonlinear features *Struct. Control Health Monit.* doi:10.1002/stc.1774